Proceedings of the ASME 2012 Summer Heat Transfer Conference
HT2012
July 8-12, 2012, Rio Grande, Puerto Rico

HT2012-58252

Simulation of Fluid Flow and Heat Transfer Including Phase Change during the Impact of Semi-Molten Particles

S. Alavi
Graduate Student
Ferdowsi University of Mashhad
Mashhad, Iran
sina.alavi@stu-mail.um.ac.ir

M. Passandideh-Fard
Associate Professor
Ferdowsi University of Mashhad
Mashhad, Iran
mpfard@um.ac.ir

J. Mostaghimi
Professor
University of Toronto
Toronto, Ontario, Canada
mostag@mie.utoronto.ca

ABSTRACT

A numerical method is proposed in this paper which is capable of modeling the impact and deposition of semi-molten particles. By attributing a high viscosity to the solid region, simulating the motion of solid cores including solidification/melting is made possible inside the particle. The Navier-Stokes equations are solved in combination with the Volume-of-Fluid (VOF) technique to track the free surface of the particles. In addition, the heat transfer including phase change is modeled using the enthalpy method. The viscous terms are treated implicitly to relax the restrictions associated with small computational time-steps in explicit formulations. Several case studies with operating conditions of a typical thermal spray process are simulated. These cases include the impact of molten and semi-molten nickel particles in an atmospheric plasma spray process (APS). The effects of various parameters such as particle solid-core diameter, initial velocity and temperature are investigated. The simulations show that the size of the solid core has an important effect on the amount of particle splashing during the impact.

KEYWORDS: Semi-molten particles, Thermal spray processes, Volume-of-Fluid (VOF), High viscosity method, Solidification and heat Transfer.

1. INTRODUCTION

Thermal spraying technology includes the coating of surfaces using different techniques to serve in several industries such as aeronautics and space industries, automotive industries, chemical and electronic industries, etc. In these techniques, molten particles are generated from raw material which is fed into a thermal spray torch, in the form of wire, rod or powder. For example in plasma spraying, a high-temperature plasma flame melts and accelerates particles, usually provided as powder, to form the coating on the substrate. The properties and microstructure of the coatings strongly depend on the phenomena happening during the particle flight time between the injection of the particles into the flame and their impact on the substrate [1]. Depending on the size and properties of the powder particles and the plasma operating conditions, such as temperature and velocity, the particles may be completely molten, completely solid or semi-molten at the impact. The presence of semi-molten particles highly increases the porosity of the final coating; as a result, the existence of these particles in a coating process is undesirable [2]. A numerical model capable of simulating this complex phenomenon, therefore, is essential in understanding various characteristics of a coating related to the impact and deposition of partially molten particles. A literature review of the research in this field explains this fact.

The history of the simulation of droplet impacts began in the late sixties when Harlow and Shannon [3] first employed the Marker-and-Cell (MAC) method in cylindrical coordinates to model the splash of droplets. Implementing heat transfer along with the fluid flow simulation during the impact was performed later by many researchers [4-7]. Brackbill et al. [8] proposed the Continuum Surface Force (CSF) model that highly improved the application of surface tension forces on the free surface. Many other aspects of the droplet impact phenomenon were studied by other researchers [9-12]. Wetting effects, droplet recoiling, convection effects, contact resistance, and droplet impacts with different velocities and temperatures on various substrates are among the studied subjects.

Later, 3D numerical simulations made possible the modeling of asymmetric phenomena like splashing and

break-up, impact on inclined substrates and the impact of droplets onto previously solidified splats [13-16]. In addition, some researchers turned their attention to other aspects of the technology including variable material properties [17, 18]. Zhang et al. [19] used the Smoothed Particle Hydrodynamics (SPH) method to model droplet splashing and spreading including solidification. Using the same method, they subsequently investigated the effects of substrate melting [20]. Moreover, Parizi et al. [21] added patterned substrates to their simulations and experiments.

Although the impact of fully molten particles has been widely studied in the literature, the publications devoted to the impact and deposition of semi-molten particles are rare. In the conventional methods for treating the solidified region, mostly known as the zero-velocity schemes, the velocity of the liquid is instantly set to zero when solidified. Another method proposed by Voller and Prakash [22] employs a source term in the momentum equations which gradually decreases the velocity of the solidifying regions until a complete solidification. The famous commercial software FLUENT utilizes this method in the problems including solidification. All of these methods are unable to model the motion of solid particles inside the main body of fluid.

Wu et al. [2] reported the existence of solid portions in the Yttria Stabilized Zirconia (YSZ) coatings. They developed a numerical method to model the impact of semi-molten droplets using the Immersed Boundary (IB) method. Their idealized model only solves for the fluid flow over the solid core which is at rest during the simulation. To simplify the problem, they have excluded the heat transfer and solidification formulations from their numerical approach. As a result, the movement of the solid core inside the liquid region and possible changes of the core due to melting/solidification are not modeled. Another approach proposed by Zirari et al. [23] uses the Specific Heat Method (SHM) in combination with the VOF technique to study the impact of semi-molten aluminum particles. Their investigation is limited to a few case studies where a large discrepancy is observed between the results of simulations and those of the experiments for droplet spreading. Furthermore, the initial conditions of the particles at the moment of impact are selected arbitrarily. Tabbara and Gu [24] proposed another method for the impingement of semi-molten particles. They used the ANSYS-FLUENT 12 software in conjunction with mesh adaptation techniques to model the solidification and deposition of semi-molten zirconia. However, the size of the solid core in their simulations is undeformed; i.e., no melting/solidification occur inside the solid core region. In addition, at each time-step of the simulation, the mesh surrounding the solid core is modified and updated to find the new position of the solid core. This treatment enables the simulation of solid-core movement inside the melt in expense of long computational times.

In this study, an in-house numerical method is presented for modeling the impact and deposition of semi-molten particles where all the various aspects associated with this phenomenon are taken into account from the onset of particle injection in the torch exit to the very last stages of particle deposition on the substrate. The momentum equations along with the energy equation are solved in an axisymmetric domain in combination with the VOF technique to track the free surface of the particles. The solid regions of the particle are treated like a liquid with high viscosity. Using a simplified analytical method, the initial state of the particle at the moment of impact is obtained to perform simulations based on educated predictions. The effects of various parameters such as particle solid-core diameter, initial velocity and temperature are also investigated.

2. NUMERICAL METHOD

2.1. Fluid flow

The Navier-Stokes equations are solved in a 2D axisymmetric domain to simulate the impact of droplets. Considering the flow to be incompressible, laminar and Newtonian, the continuity and N-S equations will become:

$$\nabla \cdot \vec{u} = 0 \tag{1}$$

$$\frac{\partial \vec{u}}{\partial t} + \nabla \cdot (\vec{u}\vec{u}) = -\frac{1}{\rho}\nabla P + \frac{1}{\rho}\nabla \cdot \vec{\tau} + \frac{1}{\rho}\vec{F}_b \tag{2}$$

in which $\vec{u}$ is the velocity vector, ρ the density, μ the dynamic viscosity, P the pressure and $\vec{\tau}$ is the stress tensor defined as:

$$\vec{\tau} = \mu[(\nabla \vec{u}) + (\nabla \vec{u})^T] \tag{3}$$

The body forces $\vec{F}_b$ include the gravity and surface tension forces. A three-step projection method [25] is employed to solve the continuity and momentum equations simultaneously in three fractional steps. In this manner, the first step includes obtaining an interim velocity $\vec{u}^{\,n+\frac{1}{3}}$ by discretizing the convective and body force terms explicitly, as follows:

$$\frac{\vec{u}^{\,n+\frac{1}{3}} - \vec{u}^{\,n}}{\delta t} = -(\vec{u} \cdot \nabla \vec{u})^n + \frac{1}{\rho^n}\vec{F}_b^n \tag{4}$$

As mentioned before, the solidified region in this study is modeled as a fluid region with a high viscosity. Therefore, the viscous terms cannot be descretized explicitly because this treatment leads to very low time-steps due to a linear stability time-step constraint [26]. Consequently, by employing implicit discretization for viscous terms, a second interim velocity is obtained in the next step as:

$$\frac{\vec{u}^{\,n+\frac{2}{3}} - \vec{u}^{\,n+\frac{1}{3}}}{\delta t} = \frac{1}{\rho^n}\nabla \cdot \left[\mu\left[\left(\nabla \vec{u}^{\,n+\frac{2}{3}}\right) + \left(\nabla \vec{u}^{\,n+\frac{2}{3}}\right)^T\right]\right] \tag{5}$$

Since the interim velocity $\vec{u}^{\,n+\frac{2}{3}}$ exists at both sides of the relation, the method of TDMA (Tri-Diagonal Matrix Algorithm) is used to obtain the interim velocity at this step.

Finally, in the third step, the interim velocity $\vec{u}^{\,n+\frac{2}{3}}$ is projected to a divergence-free velocity field, defined as follows:

$$\frac{\vec{u}^{n+1} - \vec{u}^{n+\frac{2}{3}}}{\delta t} = -\frac{1}{\rho^n}\nabla \cdot P^{n+1} \tag{6}$$

In combination with the continuity equation, this relation yields the Pressure Poisson Equation (PPE) for the evaluation of pressure at the new time level $(n+1)$, using $\vec{u}^{n+\frac{2}{3}}$:

$$\nabla \cdot \left[\frac{1}{\rho^n}\nabla P^{n+1}\right] = \frac{\nabla \cdot \vec{u}^{n+\frac{2}{3}}}{\delta t} \tag{7}$$

The resulting set of equations is symmetric and positive definite and, therefore, the Incomplete Cholesky-Conjugate Gradient (ICCG) solver is utilized to obtain the pressure [27]. The obtained pressure is next used to calculate the final velocity at time level $(n+1)$ using Eq. 6.

2.2 Free surface tracking

The interface of the particles and surrounding gas is advected using the Volume-of-Fluid (VOF) method in a fixed Eulerian mesh. This method utilizes a scalar function f as follows:

$$f = \begin{cases} 1 & \text{inside the liquid} \\ > 0, < 1 & \text{at the free surface} \\ 0 & \text{inside the gas} \end{cases} \tag{8}$$

This function shows the fraction of a cell which is filled with liquid. Consequently, when the cell is fully occupied with liquid, the value of f will be set to unity. In contrast, an empty cell will take the value of zero, and the cells residing on the interface a value between zero and one. The values for f function are advected due the following relation:

$$\frac{\partial f}{\partial t} + \left(\vec{V} \cdot \nabla\right) f = 0 \tag{9}$$

In this equation, the Youngs PLIC algorithm is used to track the free surface of the particles [28]. Surface tension is modeled using the Continuum Surface Force (CSF) proposed by Brackbill et al. [8]. Based on this method, Aleinov and Pucket [29] suggested the following relation for the surface forces:

$$\vec{F}^{ST} = \sigma\kappa\frac{A}{V}\hat{n} \tag{10}$$

in which A is the surface area of the portion of the cell filled with liquid and V is the cell volume. σ is the surface tension and $\hat{n}$ is the unit normal directing outward the liquid, which is also used to obtain the local total curvature of the free surface as:

$$\hat{n} = \frac{\nabla f}{|\nabla f|} \tag{11}$$

$$\kappa = -\nabla \cdot \hat{n} \tag{12}$$

both defined in terms of the liquid fraction f.

2.3. Heat Transfer and Solidification:

To model heat transfer including solidification, the enthalpy method is used. In this method, instead of solving the energy equation in terms of temperature, it is formulated in terms of enthalpy. This treatment enables the latent heat of fusion to be considered in the isothermal phase change of particles. The detailed description of the enthalpy method along with the method of high viscosity for treating the solidified regions is presented in this section.

2.3.1. Heat Transfer

Assuming the viscous dissipation to be negligible and constant densities for the solid, liquid and gas phases, the energy equation may be written as [30, 31]:

$$\frac{\partial h}{\partial t} + (\vec{u} \cdot \nabla)h = \frac{1}{\rho}\nabla \cdot (k\nabla T) \tag{13}$$

in which h and T are the enthalpy and temperature, respectively, and k is the thermal conductivity. A transformation is used to change the dependency of Eq. 13 only to enthalpy [32]. Also a Kirchhoff's transformation [33] is used to take the variable conductivity out of the divergence operator. The result is as follows:

$$\begin{aligned} &\rho\frac{\partial h}{\partial t} + \rho u\frac{\partial h}{\partial x} + \rho v\frac{\partial h}{\partial y} \\ &= \left[\frac{\partial}{\partial x}\left(\Gamma\frac{\partial h}{\partial x}\right) + \frac{\partial}{\partial y}\left(\Gamma\frac{\partial h}{\partial y}\right) + \frac{\Gamma}{x}\frac{\partial h}{\partial x}\right] \\ &+ \left[\frac{\partial}{\partial x}\left(h\frac{\partial \Gamma}{\partial x}\right) + \frac{\partial}{\partial y}\left(h\frac{\partial \Gamma}{\partial y}\right) + \frac{h}{x}\frac{\partial \Gamma}{\partial x}\right] \\ &+ \left[\frac{\partial^2 S}{\partial x^2} + \frac{\partial^2 S}{\partial y^2} + \frac{1}{x}\frac{\partial S}{\partial x}\right] \end{aligned} \tag{14}$$

In this relation, Γ and S are defined as follows:

$$\begin{cases} \Gamma = \dfrac{k_s}{c_s} & S = 0 & h \le 0 & \text{solid phase} \\ \Gamma = 0 & S = 0 & 0 < h < H_f & \text{interphase} \\ \Gamma = \dfrac{k_l}{c_l} & S = -H_f\dfrac{k_l}{c_l} & h \ge H_f & \text{liquid phase} \end{cases} \tag{15}$$

Equation 14 is only used inside the liquid, i.e. when f equals one. Otherwise, there will be an incorrect diffusion of enthalpy in the computational domain between two points with the same temperature. In other regions with a volume fraction smaller than one, energy equation in terms of temperature is used:

$$\begin{aligned} &\rho c\frac{\partial T}{\partial t} + \rho cu\frac{\partial T}{\partial x} + \rho cv\frac{\partial T}{\partial y} \\ &= \frac{\partial}{\partial x}\left(k\frac{\partial T}{\partial x}\right) + \frac{\partial}{\partial y}\left(k\frac{\partial T}{\partial y}\right) + \frac{k}{x}\frac{\partial T}{\partial x} \end{aligned} \tag{16}$$

In case of droplet impacts and solidification, a thermal contact resistance is taken into account between the splat and the substrate.

2.3.2. Solidification

As indicated before, in this work a new technique is implemented to model solidification based on the method of high viscosity [25]. In order to employ this method, a scalar function β (similar to f) is defined to stand for the solidified fraction of each cell as:

$$\beta = \begin{cases} 1 & h \le 0 \quad \text{solid phase} \\ \dfrac{H_f - h}{H_f} & 0 < h < H_f \quad \text{interphase} \\ 0 & h \ge H_f \quad \text{liquid phase} \end{cases} \tag{17}$$

Using this scalar, which is obtained via the solution of enthalpy equation in the liquid, we can exactly define the solidified portion of the liquid and set the values of density, conductivity and specific heat in gas, liquid and solid regions:

$$\rho = f[(1-\beta)\rho_l + \beta\rho_s] + (1-f)\rho_g \tag{18}$$

$$1/k = f[(1-\beta)/k_l + \beta/k_s] + (1-f)/k_g \tag{19}$$

$$c = f[(1-\beta)c_l + \beta c_s] + (1-f)c_g \tag{20}$$

In the above relations, subscripts g, l, and s express the gas, liquid and solid phases, respectively. If we consider the solidified region to behave like a liquid with very high viscosity, we can simply model solidification with the aid of no additional formulations or considerations. As a result, the viscosity increases to a high value as the liquid completely solidifies. The challenge associated with this method is the selection of the relation based on which the increase of viscosity takes place. Two relations are examined here. First we assume that the viscosity increases linearly with increasing the solidification fraction β as follows:

$$\mu = [1 + c_{visc}\beta]\mu_l \tag{21}$$

where μ_l is the liquid viscosity and c_{visc} is the coefficient of viscosity by which the liquid viscosity is multiplied to give the viscosity of the solidified region. This assumption is shown schematically in Fig. 1. The value of c_{visc} should be chosen large enough to mimic the rigidity condition of the solid. The main drawback of this method is that it leads to a high viscosity in the mushy zone; i.e. the liquid in this zone will behave nearly similar to solid even in the midway of solidification.

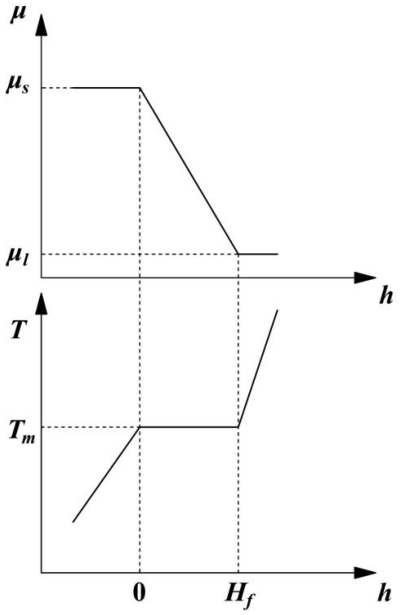

FIGURE 1. The assumption of linear variation of viscosity against enthalpy during constant-temperature solidification.

Consequently, in the second method we consider the viscosity to increase based on the following relation inspired from Voller and Prakash [22]:

$$\mu = \left[1 + c_{visc}\frac{\beta^2}{(1-\beta)^3 + \varepsilon}\right]\mu_l \tag{22}$$

where ε is a small number to prevent division by zero (set to 10^{-5} in this study). Based on this formula, the viscosity of the liquid increases slowly at the first stages of solidification and rapidly as the solidification approaches the final stages near completion. This fact is shown schematically in Fig. 2. This relation works more efficiently as we will see later in this paper. As a result, the viscosity can be expressed in the entire domain as:

$$\mu = f\mu_l + (1-f)\mu_g \tag{23}$$

in which μ_l is substituted from Eq. 22.

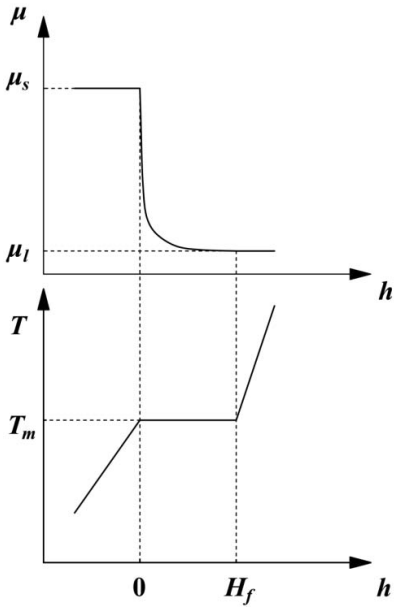

FIGURE 2. The variation of viscosity against enthalpy during constant-temperature solidification based on Eq. 22.

At this point, it should be indicated that in a pure substance, solidification occurs at a constant temperature and, therefore, no mushy zone exists. However, in the numerical method as the solid front crosses the computational mesh, the use of a mushy zone region is the only method available to model the partially-solidified cells. In this paper, therefore, when discussing the solidification mushy zone, the numerical concept is intended.

3. INITIAL STATE OF THE PARTICLE BEFORE THE IMPACT

To initialize the simulations, the initial state of the particle must be known. In this section, a simple analytical method is used to estimate the particle temperature and the size of the solid core right at the moment of impact. For this purpose, following assumptions are considered:

1. The solid region is assumed to remain at T_m during melting.

2. The problem is solved under a quasi-steady approximation.
3. The liquid region is treated under a lumped capacitance assumption.
4. Thermal properties of the solid and liquid regions are assumed to be identical.

In addition, assuming the particle to have the same velocity as of the plasma, the heat transfer coefficient h_∞ in contact with the particle, due to pure conduction, can be obtained from the following relation [34]:

$$\overline{Nu}_D = 2.0 \tag{24}$$

For the conditions of the thermal spray process, a typical APS process is used in this paper. Argon plasma discharges at 10000 K from a torch and reaches 2000 K at the substrate (adapted from Pawlowski [1]). For the purpose of this analysis, we assume the plasma temperature to decrease linearly with the distance. Since the diameter of the particles fall in the range of 44 – 120 µm as reported by Mishin et al. [35] or 60 – 80 µm as reported by Vardelle et al. [36], the assumption of lumped capacitance method is valid. Thus, in spherical coordinates, the energy equation for the particle during in-flight time is:

$$\begin{cases} \dfrac{\partial}{\partial t}\left(\rho V c T_p\right) = h_\infty A (T_\infty - T_p) \\ T_p(0) = T_0 \end{cases} \tag{25}$$

In this relation, A and V are the surface area and volume of the particle, respectively. T_p is the particle temperature, T_0 the initial temperature of the particle at the injection point, and T_∞ is the plasma temperature, respectively.

Assuming an average velocity for the particle in-flight time, therefore, the temperature of the plasma can be simplified as $T_\infty = c_1 t + c_2$ where c_1 and c_2 are to be obtained by substituting temperature values at the torch exit (10000 K) and near the substrate (2000 K). Equation 25 may now be solved as follows:

$$T_p(t) = \left(T_0 + \frac{\rho c V}{h_\infty A} c_1 - c_2\right).\exp\left(-\frac{h_\infty A}{\rho c V} t\right) + c_1 t + c_2 - \frac{\rho c V}{h_\infty A} c_1 \tag{26}$$

This relation is only valid until the particle reaches the melting point T_m; i.e. when the particle begins to release the latent heat of fusion at constant temperature. Another relation may be developed for the melting of particles in which the latent heat is taken into account:

$$\begin{cases} c_3\left(\dfrac{R_s^3 - R_p^3}{3}\right) + c_4\left(\dfrac{R_s^2 - R_p^2}{2}\right) = \left(T_m.t - \dfrac{1}{2} c_1 t^2 - c_2 t\right) \\ c_3 = \dfrac{\rho H_f}{R_p^2 h_\infty} - \dfrac{\rho H_f}{k R_p} \quad , \quad c_4 = \dfrac{\rho H_f}{k} \end{cases} \tag{27}$$

In this relation, R_s and R_p are the radii of the solid core and particle, respectively. Since R_s cannot be obtained analytically, it should be calculated via numerical treatments. A combination of Eq. 26 and Eq. 27 will help us find the state of the particle at the moment of impact on the substrate.

4. RESULTS AND DISCUSSION

To validate the numerical simulations, no experimental results were available for the impact of a semi-molten particle. Therefore, a simple analytical solution, similar to the previous section, was used. A solid nickel particle of 60 µm in diameter is assumed to be initially at the melting point. If the temperature of the free surface of the particle is kept at a value higher than the melting temperature, the particle will start to melt. Figure 3 shows a comparison between the numerical and analytical results for the variation of the solid core diameter with time, when a temperature of 1750 K is applied at the free surface. A good agreement can be seen between the numerical and analytical results which show that the solid core diameter decreases over time.

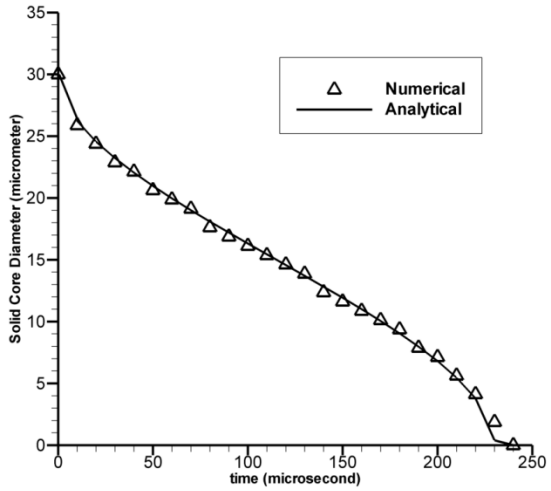

FIGURE 3. Variation of the solid core diameter against time for a nickel particle of diameter 60 µm, elapsed from the moment that a temperature of 1750 K is applied to its free surface.

The results of several simulations with various initial conditions, as listed in Table 1, are presented in this section. The typical mesh size used for the simulations consisted of about 45 cpr (cell per radius of the particle) and the typical CPU time was in the order of 20 hrs using a computer with a 2 GHz Core 2 Duo CPU. First, the results of the normal impact of a nickel particle onto a stainless steel substrate in the argon plasma environment are presented (Case 1 of Table 1).

The values for nickel, stainless steel and argon properties are given in Table 2. If the diameter of the particle is assumed to be 60 µm at 300 K, then based on the theoretical solutions of Section 3, the particle will be completely molten at the moment of impact with a temperature of 1921 K. The substrate temperature is assumed to be 1050 K and a thermal contact resistance of 10^{-6} m^2K/W is considered between the splats and the substrate (adapted from Pasandideh-Fard et al. [15]).

The evolution of the particle deformation during the impact is shown in Fig. 4. It can be seen that upon the impact, the particle starts spreading and solidifying on the substrate. Some splashing is observed after around 1 µs elapsed from the impact. The final splat is shaped as a flat disk with raised

rims. Moreover, as the streamlines in this figure illustrate, vortices are generated in the gas flow during the particle impact. These vortices influence the amount of the material detached from the particle during splashing and later control the movement of the splashed particles in-flight. This can be seen in Fig. 4 at 1 μs elapsed after the impact where in addition to the main vortex flow (generated earlier at around 0.4 μs) another circulation is observed which is caused by the movement of the splashed particle. The flat shape of the splat is desirable in thermal spray processes, since the porosity of the coating formed from the accumulation of these splats is minimal.

TABLE 1. Initial conditions of the presented simulations

Case Study		Particle diameter (μm)	Impact velocity (m/s)	Particle state	Temperature of the molten region (K)	Solid core diameter (μm)	Temperature of the solid core (K)	Substrate temperature (K)	Thermal Contact resistance (m^2K/W)
1		60	100	molten	1921	-	-	1050	10^{-6}
2		64	100	semi-molten	1737	28.7	T_m		
3	a	64	50	semi-molten	1737	28.7	T_m		
	b		100						
	c		150						
4	a	63.5	100	semi-molten	1739	18.6	T_m		
	b	64			1737	28.7			
	c	68			1733	53.4			

TABLE 2. The properties of the materials used in the simulations. The properties are taken from Incropera et al. [34], Murphy [37] and Capitelli et al. [38].

Properties / Material	Density (kg/m^3)	Thermal Conductivity $(W/m.K)$	Specific Heat $(J/kg.K)$	Dynamics Viscosity $(kg.m/s)$	Surface Tension (N/m)	Latent Heat (kJ/kg)	Melting Point (K)
Nickel	7500	80	600	0.002	1.78	297	1731.85
Stainless Steel (AISI 304)	7900	14.9	477	-	-	-	-
Argon (at 2000 K)	0.255	0.199	520.64	6.353×10^{-5}	-	-	-

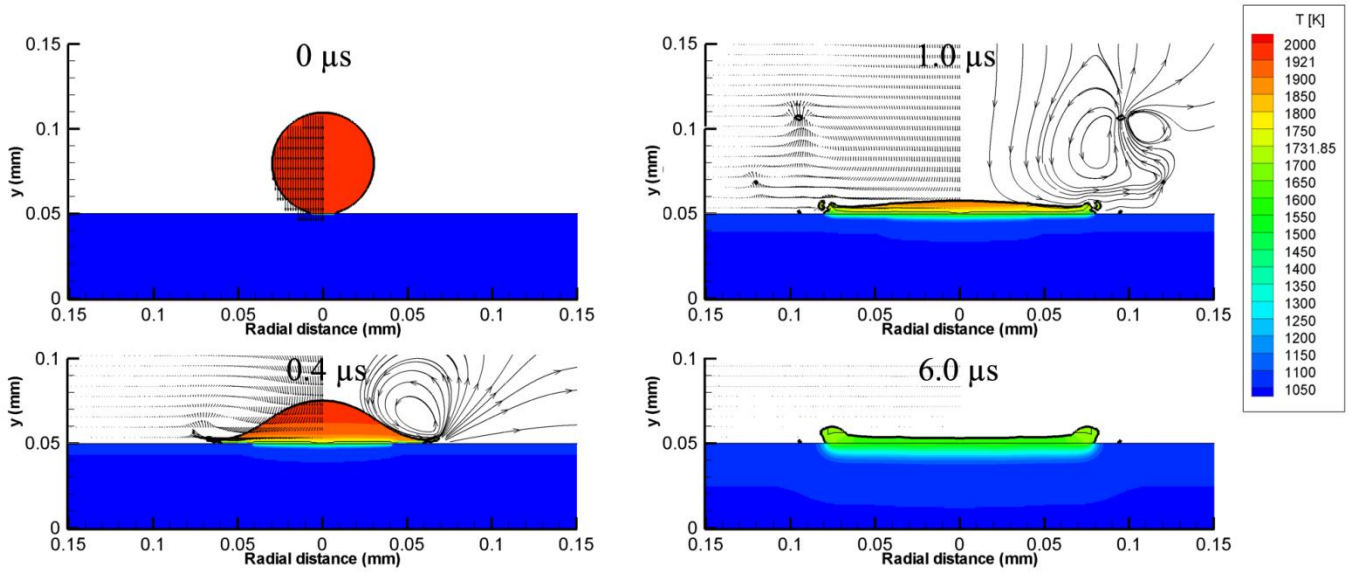

FIGURE 4. Computer-generated images of the normal impact of a nickel droplet (Case 1 of Table 1). The thin black line inside the particle shows the solidification front. See also Table 1.

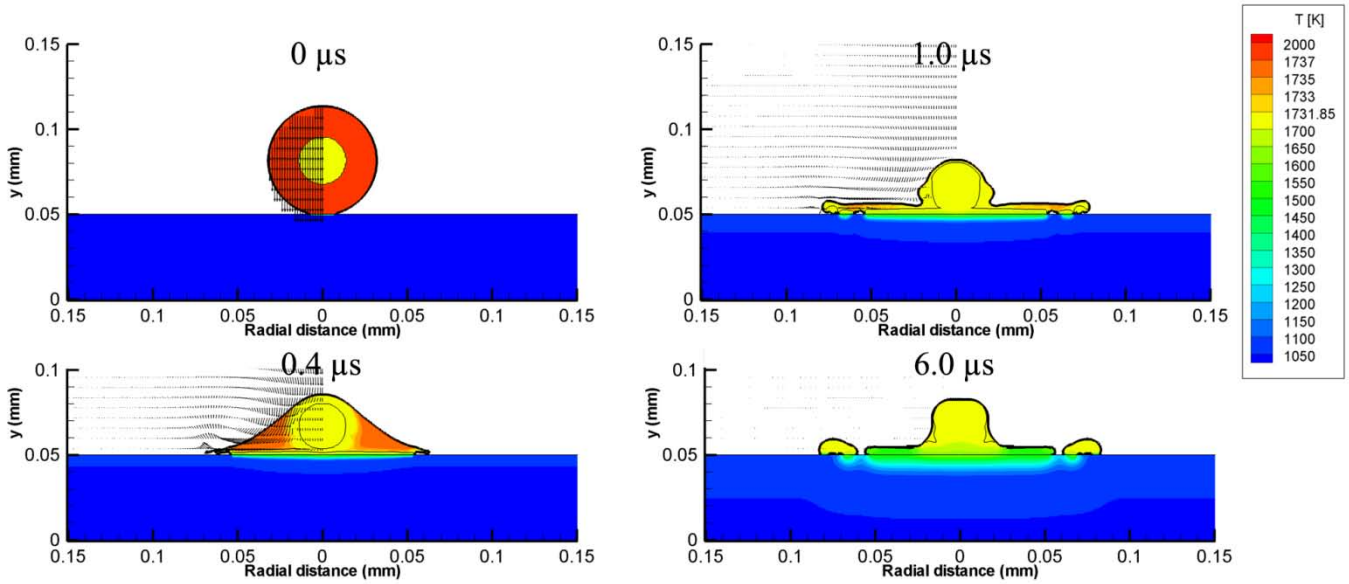

FIGURE 5. Computer-generated images of the normal impact of a semi-molten nickel particle (Case 2 of Table 1). The thin black line inside the particle shows the solidification front. See also Table 1.

For the next simulation, the initial size of the particle is assumed to be 64 μm. As the particle diameter is increased, there is no guarantee that the particle is completely molten at impact. Based on the analytical work presented in Section 3, at the moment of impact with a velocity of 100 m/s, the particle will be at 1737 K with a 28.7 μm solid core at the melting point. The phenomena happening during the impact of this particle are depicted in Fig. 5. It can be seen in this figure that in addition to a reduction in the rate of spread, there is no sign of splashing in comparison with Fig. 4 due to smaller amount of available molten material. The existence of a bump in the final splat shape is undesirable, since it initiates the formation of porosities and voids around the solid core.

To have a close inspection of the phenomena happening during the deposition of a semi-molten particle and the numerical method remarks, a magnified view of the particle is shown in Fig. 6. Based on the flow streamlines seen in Fig. 6a (0.2 μs after impact) it is evident that the solid core acts like a solid body due to its high viscosity and moves with a uniform velocity toward the substrate. As the solid core approaches the substrate it impacts on the region already being solidified on the substrate at 0.8 μs. At this time, the solid core stops against the substrate and its velocity is reduced to zero. In addition, vortices can be seen in and outside the particle. The cause of the vortex outside the particle in the gas region is the same as that for the previous case (Fig. 4). In this case, however, a clockwise vortex is observed inside the particle (in the liquid region) around and near the bottom of the solid core. This vortex, also reported by Wu et al. [2], is caused by the existence of the solid core. Due to this vortex, the portion of the melt adjacent to the solid core moves upward as seen later in the simulations. The viscosity variation presented alongside in Fig. 6 provides an insight to the rigidity of the solid core based on Eq. 22 which is a manifestation of the correctness of the value of $c_{visc} = 1000$ that leads to a rapid increase of viscosity as the material solidifies.

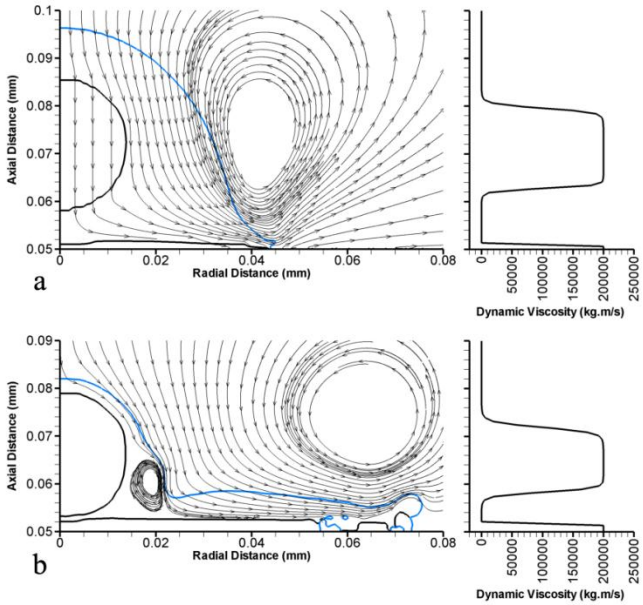

FIGURE 6. Close view of the particle impact and velocity vectors at **a)** 0.2 μs and **b)** 0.8 μs along with the variation of viscosity on the axis of symmetry, for Case 2 of Table 1 (see also Fig. 5). Solidification front is shown with a black line inside the particle.

Next case studies given in Table 1 are considered in order to investigate the effects of important parameters associated with semi-molten impacts. The effect of impact velocity is examined by three cases having the same diameter but different velocities as mentioned in Table 1 by Case 3a, 3b and 3c. Figure 7 shows the impact of semi-molten particles for these cases where the initial velocity is ranged from 50 m/s to 150 m/s. Regardless of the initial velocity of the particle, the final shape of the solidified bump seems to be similar in comparison. In contrast, the existence and amount of splashing is strongly dependent on the impact velocity as reported by many in the literature. It is evident in Fig.7 that for a particle velocity of 150 m/s, there is a significant amount of material splashing while for particles with 50 m/s and 100 m/s velocities, the splashing is not considerable. For

Case 3a with 50 m/s, the molten material spreads over the substrate very smoothly and in the recoil, part of the material breaks up from the main splat and deposits further downstream on the substrate. Figure 7 also shows that the thickness of the final splat is dependent on the impact velocity such that for Case 3b with 150 m/s, the thickness is the least. More importantly, the vortices around the solid core cause some distortions in the molten region; this is more obvious at 1.5 μs elapsed after the impact for particle with 150 m/s. The strength of these vortices depends on the impact velocity and in higher velocities may cause the melt to break up from the main body of the particle.

To study the effects of the solid core diameter on the impingement process, the size of the particle was varied from 60 μm to 68 μm. For the 60 μm particle, there was no solid core based on the analytical calculations presented in the previous section; the results for this case (Case 1 of Table 1) were presented in Fig. 4. Three other particle diameters considered for the simulations are listed as Case 4 in Table 1. The size of the solid core for these cases based on the analytical method varies from 18.6 μm for Case 4a to 53.4 μm for Case 4b. Figure 8 demonstrates the evolution of the flow deformation, heat transfer and phase change during the impact of these particles. It can be seen in this figure that as the initial particle size increases, the size of the solid core increases and, as a result, the initial temperature of the molten region decreases. Therefore, for Case 4a where more material is in the molten state, a significant amount of break-up occurs. Consequently, for a particle with less amount of the solid core, the final bump in the splat is less pronounced.

5. CONCLUSION

A new method for modeling solidification is proposed for the impact of particles in thermal spray processes. Based on the high viscosity method, the solid regions are treated like a liquid with a high viscosity. This technique is implemented into the heat transfer and fluid flow formulations. The Navier-Stokes equations are solved in an axisymmetric, fixed-grid Eulerian domain and the free surface tracking is accomplished using the Volume-of-Fluid (VOF) method. The energy equation is solved using the enthalpy method inside the particle. Combined with predictions based on the analytical calculations, this method is capable of simulating the impact and deposition of semi-molten particles with a solid core inside. Several case studies were presented to cover various possibilities of impact forms in thermal spray processes. First, the impact of a fully-molten nickel particle onto a stainless steel substrate was studied where a good agreement was obtained between the experimental and numerical results reported in the literature. Next, the impact of a particle with a solid core was investigated. Results demonstrated that a solid bump forms as a consequence of the solid core in the final splat shape. The effects of the impact velocity and the size of the solid core on the particle impingement were also investigated. The impact characteristics including splashing, bump size and amount of spread on the substrate depends on the particle velocity and the size of the solid core. It was found that the main effect of initial velocity is on the amount of particle splashing, splat thickness and vortical distortions. The size of the solid core, however, affects the final size of the bump, the spreading of the splat and the amount of splashing.

ACKNOWLEDGMENT

This work was supported by the Research Grant No. 2/19797 from the Ferdowsi University of Mashhad, Mashhad, Iran.

REFERENCES

1. Pawlowski, L., 2008, "*The Science and Engineering of Thermal Spray Coatings*," 2nd ed., Wiley, Chichester, England.
2. Wu, T., Bussmann, M., and Mostaghimi, J. (2009). "The Impact of a Partially Molten YSZ Particle," *J. Therm. Spray Technol.*, **18(5)**, pp. 957-964.
3. Harlow, F. H., and Shannon, J. P. (1967). "The Splash of a Liquid Droplet," *J. Appl. Phys.*, **38(10)**, pp. 3855-3866.
4. Tsurutani, K., Yao, M., Senda, J., and Fujimoto, H. (1990). "Numerical Analysis of The Deformation Process of a Droplet Impinging Upon a Wall," *JSME Int. Ser. II*, **33(3)**, pp. 555-561.
5. Trapaga, G., and Szekely, J. (1991). "Mathematical Modeling of The Isothermal Impingement of Liquid Droplets in Spraying Processes, "*Metall. Trans. B*, **22(6)**, pp. 901-914.
6. Sicilian, J. M., Hirt, C. W. (1988). "Flow-3D: Computational Modeling Power for Scientists and Engineers," Technical Report FSI-88-00-1, Flow Science Inc. San Diego, CA.
7. Kothe, D. B., Mjolsness, R. C., and Torrey, M. D. (1991). "RIPPLE: A Computer Program for Incompressible Flows With Free Surfaces," Technical Report LA-12007-MS, LANL. Los Alamos, NM.
8. Brackbill, J.U., Kothe, D.B., and Zemach, C. (1992). "A Continuum Method for Modeling Surface Tension, " *Journal of Computational Physics*, **100(2)**, pp. 335-354.
9. Fukai, J., Shiiba, Y., Yamamoto, T., Miyatake, O., Poulikakos, D., Megaridis, C.M., and Zhao, Z. (1995). "Wetting Effects on The Spreading of a Liquid Droplet Colliding With a Flat Surface: Experiment and Modeling," *Phys. Fluids*, **7(2)**, pp. 236-247.
10. Zhao, Z., Poulikakos, D., and Fukai, J. (1996). "Heat Transfer and Fluid Dynamics During The Collision of a Liquid Droplet on a Substrate - I. Modeling," *Int. J. Heat Mass transfer*, **39(13)**, pp. 2771-2789.
11. Waldvogel, J. M., and Poulikakos, D. (1997). "Solidification Phenomena in Picoleter Size Solder Droplet Deposition on a Composite Substrate, "*Int. J. Heat Mass Transfer*, **40(2)**, pp. 295-309.
12. Pasandideh-Fard, M., Bhola, R., Chandra, S., and Mostaghimi, J. (1998). "Deposition of Tin Droplets on a Steel Plate: Simulations and Experiments," *Int. J. Heat Mass Transfer*, **41(19)**, pp. 2929-2945.
13. Bussmann, M., Mostaghimi, J., and Chandra, S. (1999). "On a Three-Dimensional Volume Tracking Model of Droplet Impact," *Physics Fluids*, **11(6)**, pp. 1406-1417.

14. Bussmann, M., Chandra, S., and Mostaghimi, J. (2000).“ Modeling The Splash of a Droplet Impacting a Solid Surface,” *Phys. Fluids*, **12(12)**, pp. 3121-3132.
15. Pasandideh-Fard, M., Pershin, V., Chandra, S., and Mostaghimi, J. (2002). “Splat Shapes in a Thermal Spray Coating Process: Simulation and Experiments,” *J. Thermal Spray Technol.*, **11(2)**, pp. 206-217.
16. Pasandideh-Fard, M., Chandra, S., and Mostaghimi, J. (2002). “A Three-Dimensional Model of Droplet Impact and Solidification,” *Int. J. Heat Mass Transfer*, **45(11)**, pp. 2229-2242.
17. Raessi, M., and Mostaghimi, J. (2005). “Three-Dimensional Modeling of Density Variation Due to Phase Change in Complex Free Surface Flows,” *Numerical Heat Transfer B: Fundamentals*, **47(6)**, pp. 507-531.
18. Alavi, S., and Passandideh-Fard, M. (2011). “Numerical Simulation of Droplet Impact and Solidification including Thermal Shrinkage in a Thermal Spray Process,” *Frontiers in Heat and Mass Transfer*, **2(2)**.
19. Zhang, M.Y., Zhang, H., andZheng, L.L. (2008). “Simulation of Droplet Spreading, Splashing and Solidification Using Smoothed Particle Hydrodynamics Method,” *Int. J. Heat Mass Transfer*, **51(13-14)**, pp. 3410-3419.
20. Zhang, M., Zhang, H., and Zheng, L. (2009). “Numerical Investigation of Substrate Melting and Deformation During Thermal Spray Coating by SPH Method,” *Chemistry and Materials Science*, **29(1)**, pp. 55-68.
21. Parizi, H.B., Rosenzweig, L., Mostaghimi, J., Chandra, S., Coyle, T., Salimi, H., Pershin, L., McDonald, A., and Moreau, C. (2007). “Numerical Simulation of Droplet Impact on Patterned Surfaces,” *J. Therm. Spray Technol.*, **16(5-6)**, pp. 713-721.
22. Voller, V. R., and Prakash, C. A. (1987). “Fixed-Grid Numerical Modeling Methodology for Convection-Diffusion Mushy Region Phase-Change Problems,” *Int. J. Heat Mass Transfer*, **30(8)**, pp. 1709-1720.
23. Zirari, M., Abdellah El-Hadj, A., Bacha, N. (2010). “Numerical Analysis of Partially Molten Splat During Thermal Spray Process Using The Finite Element Method, ” *Applied Surface Science*, **256(11)**, pp. 3581-3585.
24. Tabbara, H., and Gu, S. (2011). “Numerical Study of Semi-Molten Droplet Impingement,” *Physics and Astronomy*, **104(4)**, pp. 1011-1019.
25. Mirzaii, I., and Passandideh-Fard, M. (2011). “Modeling free surface flows in presence of an arbitrary moving object,” *Int. J. Multiphase Flow*, (in press).
26. Harlow, F.H., and Amsden, A.A. (1971). “Fluid dynamics: A LASL monograph (Mathematical solutions for problems in fluid dynamics),” LA 4700, Los Alamos National Laboratory.
27. Kershaw, D.S. (1978). “The Incomplete Cholesky-Conjugate Gradient Method for the Iterative Solution of Systems of Linear Equations,” *Journal of Computational Physics*, **26(1)**, pp. 43-65.
28. Youngs, D.L. (1984). “An Interface Tracking Method for a 3D Eulerian Hydrodynamics Code,” Technical report 44/92/35, AWRE.
29. Aleinov, I., and Puckett, E.G. (1995). “Computing Surface Tension With High-Order Kernels,” *Sixth International Symposium on Computational Fluid dynamics*, Lake Tahoe, NV, pp. 13-18.
30. Carslaw, H.S. and Jaeger, J. C. (1975). “*Conduction of Heat in Solids*,” Oxford University Press, London.
31. Shamsunder, N. and Sparrow, E.M. (1975). “Analysis of Multidimensional Conduction Phase Change via the Enthalpy Model,” *J. Heat Transfer*, **97(3)**, pp. 333-340.
32. Cao, Y., Faghri, A. and Chang, W.S. (1989). “A Numerical Analysis of Stefan Problems for Generalized Multi-Dimensional Phase-Change Structures Using The Enthalpy Transforming Model,” *Int. J. of Heat Mass Transfer*, **32(7)**, pp. 1289-1297.
33. Solomon, A.D., Morris, M.D., Martin, J. and Olszewski, M. (1986). “The Development of a Simulation Code for a Latent Heat Thermal Energy Storage System in a Space Station,” Technical Report ORNL-6213.
34. Incropera, F. P., DeWitt, D. P., Bergman, T. L. and Lavine, A. S. (2007). “*Introduction to Heat Transfer*,” 5th ed., John Wiley and Sons, New York.
35. Mishin, J., Vardelle, M., Lesinski, J., and Fauchais, P. (1985). “Measurement of Surface Temperature of Particles Sprayed By DC Plasma Jet by Color Pyrometry in Flight,” *7th International Symposium on Plasma Chemistry*, Eindhoven, Netherlands, pp. 724-729.
36. Vardelle, M., Vardelle, A., and Fauchais, P. (1989). “Etude Comparative Du Traitement Thermique Des Poudres en Projection Plasma a L’airet en Atmosphere Controlee (Comparative Study between Thermal Treatment of Powders Sprayed in Air or in Controlled Atmosphere Plasma),” *Revue Internationale de Hautes Temperatures et Refractaires*, **25(2)**, pp. 83-91 (in French).
37. Murphy, A. B. (2000). “Transport Coefficients of Hydrogen and Argon–Hydrogen Plasmas,” *Plasma Chemistry and Plasma Processing*, **20(3)**, pp. 279-297.
38. Capitelli, M., Fiocelli, E., and Molinari, E. (1972). “Equilibrium Compositions and Thermodynamics Properties of Mixed Plasmas,” University of Bari, Bari, Italy, report available upon request.

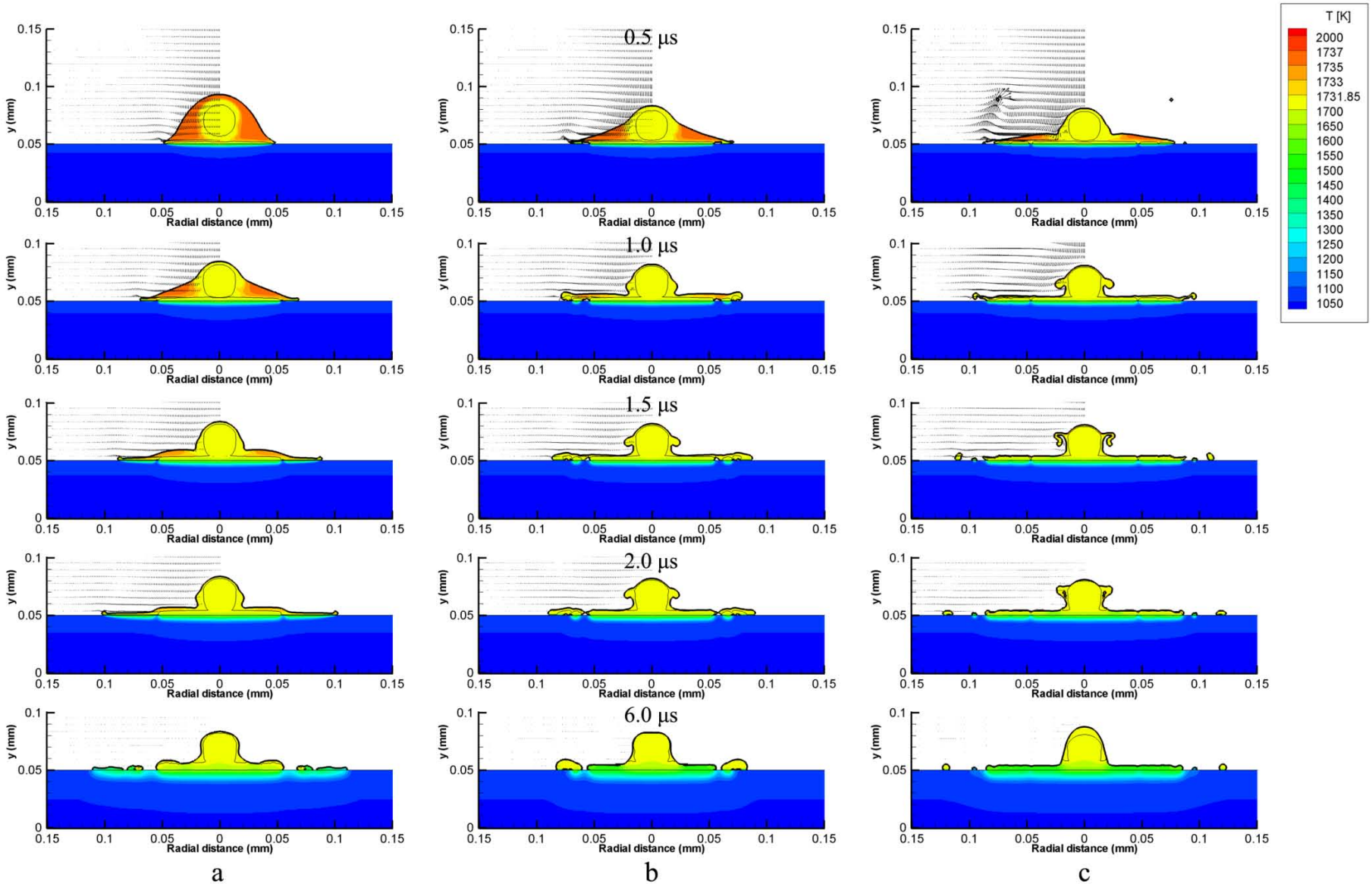

FIGURE 7. Comparison between the impacts of 64 μm dia. semi-molten nickel particles with a velocity of **a)** 50 m/s (Case 3a of Table 1); **b)** 100 m/s (Case 3b of Table 1); and **c)** 150 m/s (Case 3c of Table 1). The thin black line inside the particles shows the solidification front.

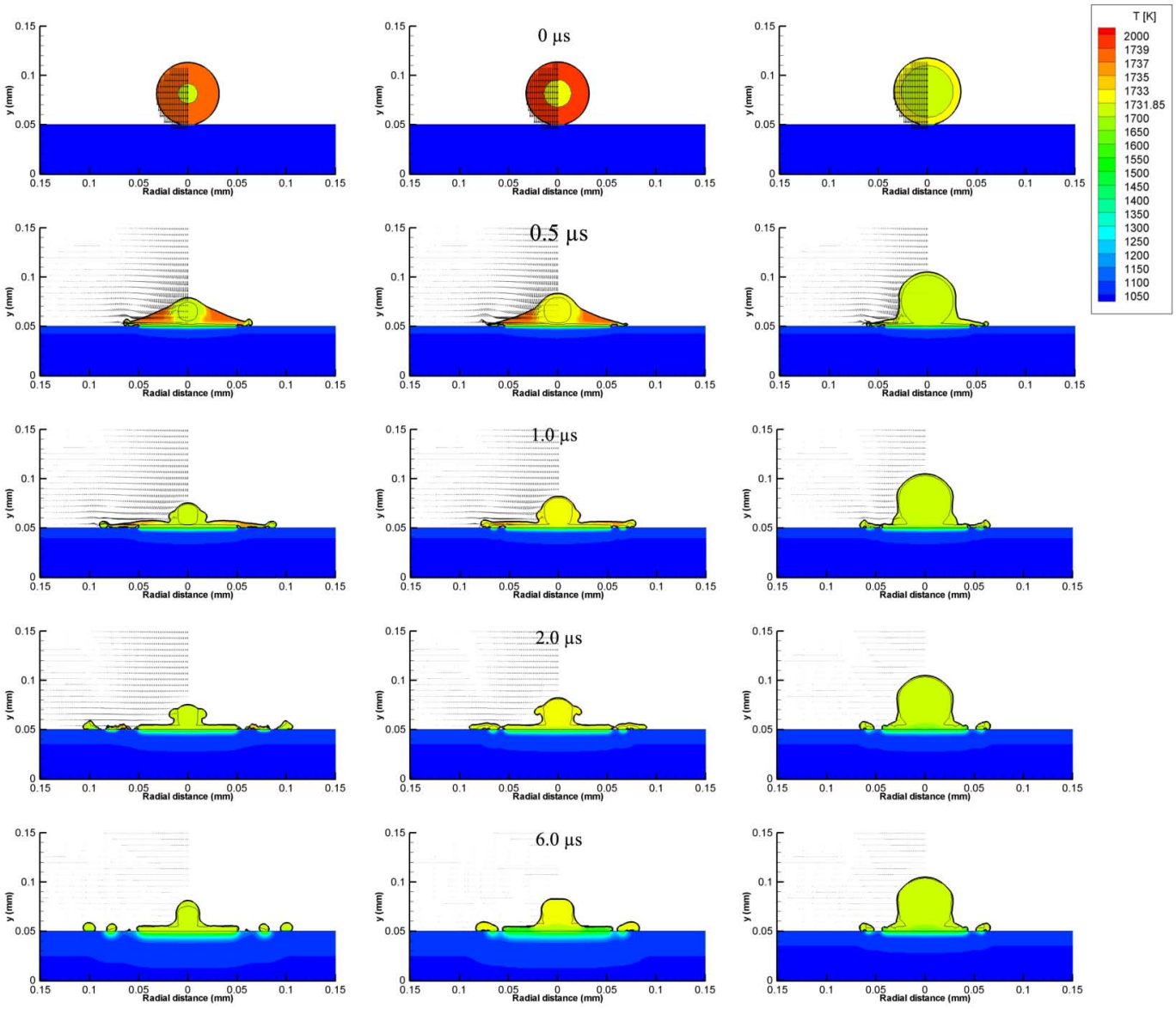

FIGURE 8. Comparison between the impacts of semi-molten nickel particles with **a)** 63.5 µm dia. (Case 4a of Table 1); **b)** 64 µm dia. (Case 4b of Table 1); and **c)** 68µm dia. (Case 4c of Table 1) for a 100 m/s velocity. The thin black line inside the particles shows the solidification front.